Victor H. Perez-Gonzalez

Tecnologico de Monterrey, School of Engineering and Sciences, Monterrey, Mexico

Received April 29, 2021
Revised May 29, 2021
Accepted June 1, 2021

Review

Particle trapping in electrically driven insulator-based microfluidics: Dielectrophoresis and induced-charge electrokinetics

Electrokinetically driven insulator-based microfluidic devices represent an attractive option to manipulate particle suspensions. These devices can filtrate, concentrate, separate, or characterize micro and nanoparticles of interest. Two decades ago, inspired by electrode-based dielectrophoresis, the concept of insulator-based dielectrophoresis (iDEP) was born. In these microfluidic devices, insulating structures (i.e., posts, membranes, obstacles, or constrictions) built within the channel are used to deform the spatial distribution of an externally generated electric field. As a result, particles suspended in solution experience dielectrophoresis (DEP). Since then, it has been assumed that DEP is responsible for particle trapping in these devices, regardless of the type of voltage being applied to generate the electric field—direct current (DC) or alternating current. Recent findings challenge this assumption by demonstrating particle trapping and even particle flow reversal in devices that prevent DEP from occurring (i.e., unobstructed long straight channels stimulated with a DC voltage and featuring a uniform electric field). The theory introduced to explain those unexpected observations was then applied to conventional "DC-iDEP" devices, demonstrating better prediction accuracy than that achieved with the conventional DEP-centered theory. This contribution summarizes contributions made during the last two decades, comparing both theories to explain particle trapping and highlighting challenges to address in the near future.

Keywords:
Dielectrophoresis / Electrokinetics / Electrophoresis / Lab-on-a-chip / Microfluidics
DOI 10.1002/elps.202100123

1 Introduction

Dielectrophoresis (DEP), the force acting on polarizable matter subjected to a nonuniform electric field, has been extensively used to manipulate and characterize a wide range of micro- and nano- particles [1]. Mammalian cells [2], viruses [3], bacteria [4], yeast [5], microalgae [6], DNA [7], and RNA [8] have been studied through DEP. This interesting electrokinetic (EK) technique, from its conception, has been associated with a pair of electrodes differing in size or shape upon which a direct current (DC) or alternating current (AC) voltage is applied to generate a nonuniform electric field [9]. Such an approach to DEP is known as electrode-based DEP (eDEP). Professor Herbert Pohl first described DEP through a careful experimental setup that included two small electrodes (quite large electrodes for the current standard of the technology) that created a radially distributed electric field [10]. Later, because of significant improvements in micro- and nanofabrication tools and protocols, dimensions shrank considerably. The reduced electrode size allowed generating highly nonuniform electric field distributions, and the microfabrication techniques allowed integrating those electrodes within microfluidic devices [11]. With this, it became possible to start probing the DEP response of the many particles listed above.

Many motivations exist for working in the microfluidic field [12]. However, one that is particularly interesting for the DEP community is the possibility to develop Point-of-Care (POC) or Lab on a Chip (LOC) devices. These devices would be taken to low-income communities with no access to clinical laboratories for immediate and reliable diagnosis of illnesses. To truly serve this purpose, POC devices must be portable, disposable, and low-cost. Also, these devices must

Correspondence: Dr. Victor H. Perez-Gonzalez, Department of Mechatronics and Electrical Engineering, Tecnologico de Monterrey, Monterrey, NL 64849, MX
E-mail: vhpg@tec.mx

Abbreviations: **AC**, alternating current; **cDEP**, contactless dielectrophoresis; **DC**, direct current; **DEP**, dielectrophoresis; **eDEP**, electrode-based dielectrophoresis; **EDL**, electric double layer; **EK**, electrokinetic; **EO**, electroosmosis; **EP**, electrophoresis; **iDEP**, insulator-based dielectrophoresis; **LOC**, lab on a chip; **POC**, point of care; **rDEP**, reservoir-based dielectrophoresis

Color online: See article online to view Figs. 1–5 in color.

not require excessive peripheral bulky instrumentation (e.g., power sources, syringe pumps, microscopes, potentiostats, etc.). Otherwise, the device would be better described as a "Chip in a Lab" and not as a "Lab on a Chip". Electrode-based DEP devices generally require syringe pumps to drive fluid motion [13]; their fabrication process is lengthy, cumbersome, and expensive [14]; and they incur in significant Joule Heating [15]. Because these features of eDEP are not amenable for developing LOC devices, different approaches to induce DEP were sought. It was under these circumstances that attention was paid to insulators.

Insulator-based technology originally relied on using insulating structures—embedded within a microfluidic device—to distort an otherwise uniform electric field, inducing DEP in particles suspended therein [16]. These devices can be fabricated using different approaches including photolithography + soft lithography, CNC milling, and xurography, all of which can be carried out outside cleanroom facilities, significantly lowering fabrication costs. As these devices do not require integrated metallic electrodes, they can be more easily disposed after use. Also, if a DC voltage is applied across the channel using external electrodes, two additional things will happen: (1) a net electroosmotic flow (EOF) will be generated within, eliminating the requirement of an external syringe pump to drive fluid motion and drag particles along from the inlet to the outlet; and (2) a net electrophoretic (EP) component of particle velocity will develop, which may act in an opposite direction to that of electroosmosis, collaborating with DEP in trapping particles [17]. All these attractive features launched the insulator-based dielectrophoresis (iDEP) term into scientific stardom [18].

Over the years, the iDEP community has produced several successful branches of the technique (contactless dielectrophoresis [cDEP], reservoir-based dielectrophoresis [rDEP], curvature-induced dielectrophoresis, gradient iDEP, etc.), all based on the fundamental principle of using insulators to distort the spatial distribution of an electric field and exploit DEP to control particle movement [19–22]. Some of these iDEP variants work in the DC regime and some work in the AC one. Nonetheless, recent findings suggest that the classic theory of DEP might be unable to accurately describe particle manipulation in insulator-based devices operating under DC conditions. In 2020, Cardenas-Benitez et al. successfully demonstrated that this scenario is better described by an equilibrium between linear and nonlinear electrophoresis and electroosmosis, and that the contribution of DEP to particle manipulation is so small it can be, in general, discarded [23]. This finding must lead to a change in our vocabulary to refer to this field; because if DEP is a negligible force, the DC-iDEP devices might be better referred to as DC insulator-based electrokinetic (DC-iEK) devices. Moreover, a rising theory published in 2018 states that, for proteins and other polar molecules, permanent dipoles can lead to a DEP force orders of magnitude larger than that predicted by the classical DEP theory in the AC regime [24]. These findings—and others to be discussed herein—represent the promising present of this research field, which is filled with potential to tackle new applications and address new challenges.

This review will provide a historical overview of the insulator-based electrokinetic (iEK) research field. Section 2, Background, will provide the necessary basic theory for the non-expert reader. Following this, Section 3, Insulator-based Dielectrophoresis (iDEP), will discuss the origins of the research field and contributions where DEP was considered the dominant mechanism behind particle manipulation and characterization—in both DC and AC fields. Then, Section 4, DC-Insulator-based Electrokinetics (DC-iEK), will describe recent findings that have the potential to change our perspective of this technology. After that, challenges to address will be outlined in Section 5, Future Perspectives and Concluding Remarks.

2 Background

2.1 Electrical

Electrokinetic phenomena occur because of the interaction of electric charges with an electric field and can be traced back to Coulomb's Law. Depending on the charge distribution present in a channel-liquid-particle system and the properties of the externally generated electric field (DC versus AC and uniform versus nonuniform) different EK techniques can be exploited to drive fluid and particle motion [25]. Moreover, other electrically-driven phenomena (e.g., electrolysis and Joule Heating) might also be present in an iEK experiment [26,27]. This section briefly describes the basic fundamentals behind electrically-driven phenomena acting in iEK devices.

2.1.1 Dielectrophoresis (DEP)

To describe DEP, consider a homogeneous spherical particle suspended in a liquid. Both the particle and liquid feature different dielectric properties (i.e., electrical conductivity and permittivity), and an electric field is applied across the suspension. As a response to the electric stimulus, charges in the system will redistribute themselves. At the particle/liquid interface, two electric dipoles will be induced (Maxwell-Wagner interfacial polarization [9]). The electric dipole induced on the particle side of the interface is due to the free and bound charges of the particle. The electric dipole induced on the liquid side of the interface is due to the accumulation of counterions therein—this is known as the Electrical Double Layer (EDL); consult [1,12,25] for details. Both these dipoles point in opposite directions and combine to produce a net dipole moment, which will interact with the electric field that induced it. If the field is uniform, the force acting on one side of the net dipole will be balanced by that acting on the other side, and the particle will not move (hence, no DEP). In contrast, if the field is nonuniform, we must carefully consider which of the two induced dipoles is dominant (that on the particle side of the interface or that on the liquid side of the interface). If the particle is more polarizable than its suspending

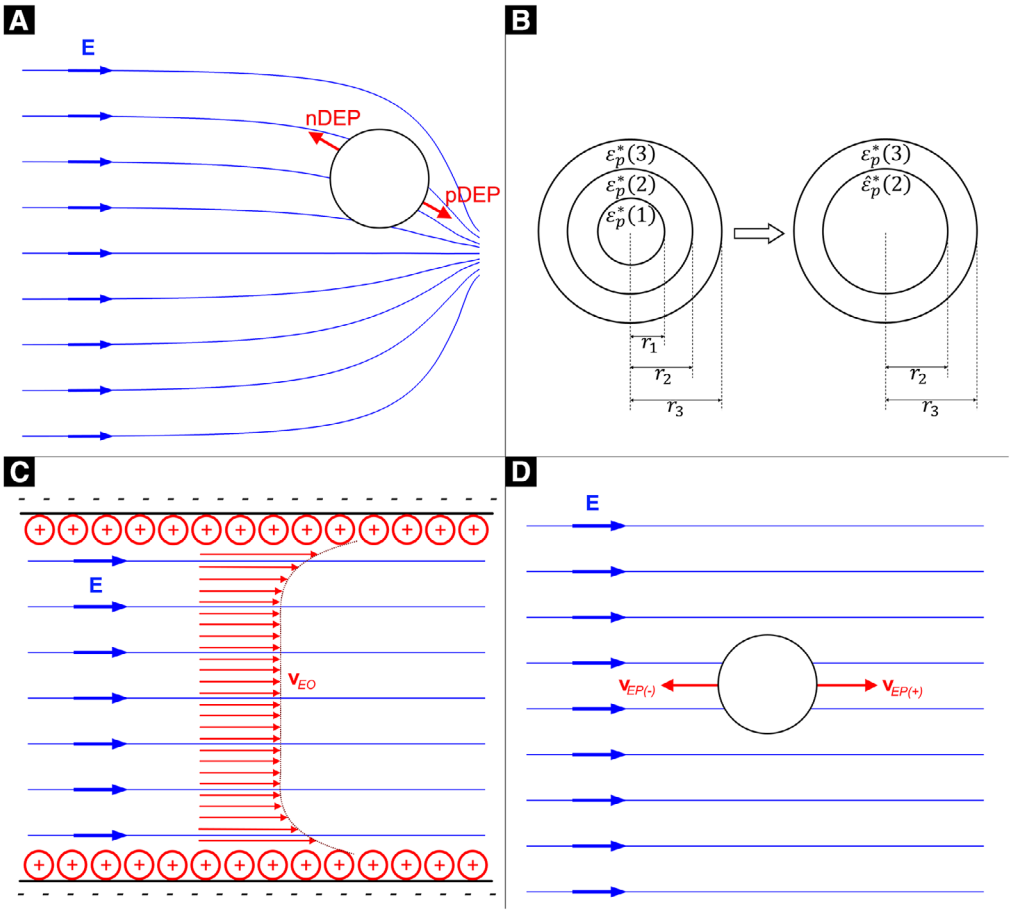

Figure 1. Schematic diagrams of the multishell particle model and basic electrokinetic phenomena present in iEK microfluidic devices. **(A)** Dielectrophoresis (DEP); a homogeneous spherical polarizable particle suspended in a fluid and subjected to a nonuniform electric field is attracted to regions where the electric field is highly nonuniform when it is more polarizable than the fluid (pDEP), or it is repelled from those regions when it is less polarizable than the fluid (nDEP). **(B)** Multishell model; used to study the dielectric properties of cells. In the case depicted in the figure, three spherical layers are considered—i.e., cytoplasm (1), membrane (2), and wall (3)—each with its own set of dielectric properties. Using Eq. (4), an equivalent set of dielectric properties is obtained for the whole particle. **(C)** Electroosmosis (EO); an ion-containing liquid is in contact with a charged surface in the presence of an external electric field. A layer of counterions forms at the surface/liquid interface and responds to the electric field by moving. The liquid moves in the direction of the electric field for negatively charged surfaces, and it moves in the direction opposite to the field for positively charged surfaces. **(D)** Electrophoresis (EP); a charged particle suspended in a fluid is subjected to an electric field and responds by moving. If the particle is positively charged, it will exhibit a positive electrophoretic mobility and move in the direction of the field ($\mathbf{v}_{EP(+)}$). If the particle is negatively charged, it will exhibit a negative electrophoretic mobility and move in the direction opposite to the field ($\mathbf{v}_{EP(-)}$).

solution, the electric dipole on the particle side of the interface will dominate. In this case, the orientation of the net dipole and that of the electric field will be parallel, and the particle will be attracted towards those regions where the field is highly nonuniform (positive DEP or pDEP). If the suspending solution is more polarizable than the particle, the electric dipole on the liquid side of the interface will dominate. In this case, the orientation of the net dipole and that of the electric field will be antiparallel, and the particle will be repelled from those regions where the field is highly nonuniform (negative DEP or nDEP) [9]. Both these scenarios are depicted in Fig. 1A. The DEP force acting on a homogeneous spherical particle is given by the expression:

$$\mathbf{F}_{DEP}\ (\omega) = 2\pi a^3 \varepsilon_m \mathrm{Re}\{K\} \nabla (\mathbf{E}_{RMS} \cdot \mathbf{E}_{RMS}) \quad (1)$$

where a represents the radius of the sphere; ε_m is the permittivity of the suspending solution; $\mathbf{E}_{RMS}$ is the RMS value of the electric field vector $\mathbf{E}$; ω is the angular frequency of $\mathbf{E}$; Re{ } is the real operator; and K is the complex Clausius–Mossotti factor:

$$K = \frac{\varepsilon_p^* - \varepsilon_m^*}{\varepsilon_p^* + 2\varepsilon_m^*} \quad (2)$$

with $\varepsilon_i^* = \varepsilon_i - j\sigma_i/\omega$; where ε^* is the complex permittivity; ε stands for permittivity (the product of the permittivity of free space, ε_0, and the dielectric constant of the material); σ represents electrical conductivity; and the subscript i is p for particle and m for suspending solution. In Eqn. (1), $-0.5 \leq \mathrm{Re}\{K\} \leq 1$, giving rise to pDEP if $\mathrm{Re}\{K\} > 0$ (i.e., the particle is more polarizable than the suspending solution),

nDEP if Re{K} < 0 (i.e., the suspending solution is more polarizable than the particle), and no DEP if Re {K} = 0 (i.e., particle and solution are equally polarizable). When, for a certain value of ω, Re {K} = 0, a crossover angular frequency (that one for which pDEP turns into nDEP or where nDEP turns into pDEP [28]) can be defined from Eqn. (2) as:

$$\omega_x = \left(\frac{\sigma_p^2 + \sigma_p \sigma_m - 2\sigma_m^2}{\varepsilon_p^2 + \varepsilon_p \varepsilon_m - 2\varepsilon_m^2} \right)^{1/2} \tag{3}$$

Moreover, if the particle is not homogeneous (e.g., a cell that embodies a cytoplasm, a membrane, and a wall), a multishell model can be used to calculate $\hat{\varepsilon}_p^*$, the equivalent complex particle permittivity [9].

$$\hat{\varepsilon}_p^*\ (n+1) = \varepsilon_p^*\ (n+1) \left[\frac{b^3 + 2\left(\frac{\hat{\varepsilon}_p^*(n) - \varepsilon_p^*(n+1)}{\hat{\varepsilon}_p^*(n) + 2\varepsilon_p^*(n+1)} \right)}{b^3 - \left(\frac{\hat{\varepsilon}_p^*(n) - \varepsilon_p^*(n+1)}{\hat{\varepsilon}_p^*(n) + 2\varepsilon_p^*(n+1)} \right)} \right] \tag{4}$$

In Eqn. (4), for a particle with N shells, n (the shell index) varies from 1 to $N-1$; also, $\hat{\varepsilon}_p^*\ (1) = \varepsilon_p^*\ (1)$; and $b = a_{n+1}/a_n$ (see Fig. 1B). Once $\hat{\varepsilon}_p^*(N)$ has been calculated, it will substitute ε_p^* in Eqn. (2).

Because of the suspending solution viscosity, η, a spherical particle subjected to a DEP force (and in the absence of other forces) will acquire a velocity $\mathbf{v}_{DEP} = \mu_{DEP}\ \nabla(\mathbf{E}_{RMS} \cdot \mathbf{E}_{RMS})$, where μ_{DEP} represents the DEP mobility, which is given by:

$$\mu_{DEP} = \frac{a^2 \varepsilon_m \mathrm{Re}\{K\}}{3\eta} \tag{5}$$

For particles with different geometries, the reader is referred to [29].

2.1.2 Electroosmosis (EO)

To describe EO, consider a charged surface in contact with an ion-containing liquid. In this case, the charged surface can be a microfluidic channel wall [e.g., polydimethylsiloxane (PDMS) is negatively charged]. At the surface/liquid interface, an EDL will form mostly containing counter-ions to mirror the surface charge [12]. In the presence of an electric field—applied via an external set of electrodes stimulated by a DC or AC power source—the EDL will interact with it, resulting in EDL displacement (i.e., it will experience EO). If the EDL is mostly composed of negative ions, it will move in the direction opposite to the electric field; in contrast, if composed of positive ions, it will move in the direction established by the electric field. Because of the viscous effects, the bulk of liquid will be dragged along the direction of EDL displacement as shown in Fig. 1C.

For simplicity, let us assume a simple case where the electric field only has an x-component (i.e., $\mathbf{E} = E_x\ \mathbf{a}_x$) so that the linear electroosmotic velocity can be described as a scalar field by the expression:

$$v_{EO} = \mu_{EO}\ E \tag{6}$$

where μ_{EO} is the electroosmotic mobility, given by:

$$\mu_{EO} = -\frac{\varepsilon_m \zeta_w}{\eta} \tag{7}$$

with ζ_w representing the zeta potential of the surface (i.e., the electric potential at the slip plane of the EDL; the reader is referred to [1] for details). ζ_w is positive for positively charged surfaces and negative for negatively charged surfaces. Therefore, according to Eqns. (6) and (7), the fluid flow follows the electric field for negatively charged surfaces and goes against it for positively charged ones. In the case of stimulation with an AC voltage, zero time average EO results.

2.1.3 Electrophoresis

To describe EP, consider a charged particle suspended in an ion-containing liquid. This scenario can be analyzed in the same terms used above for EO. Again, an EDL will form (this time around the particle), characterized by a zeta potential of its own, ζ_p, which will be positive for a positively charged particle, and negative for a negatively charged one [12]. In the presence of an externally generated DC or AC electric field, the particle will move relative to the fluid (i.e., it will experience EP).

Assuming, once more, that the electric field only has an x-component, the linear electrophoretic velocity can then be described by the scalar expression:

$$v_{EP} = \mu_{EP}\ E \tag{8}$$

where μ_{EP} is the electrophoretic mobility, given by:

$$\mu_{EP} = \frac{\varepsilon_m \zeta_p}{\eta} \tag{9}$$

It follows then, from Eqns. (8) and (9), that positively charged particles move in the direction of the electric field and negatively charged particles move against the field (see Fig. 1D). In the case of stimulation with an AC voltage, zero time average EP results.

2.1.4 Electrolysis

In the context of iEK devices, electrolysis, defined as the use of an electric current to stimulate a non-spontaneous reaction, can have a significant and adverse effect [14]. Consider a set of platinum wires (electrodes) immersed in the inlet and outlet reservoirs of a DC-iEK device filled with water. Commonly, devices of this type operate with voltages ranging from a few tens of volts to a few thousands of volts, depending on the application. Water requires a minimum voltage of 1.23 V to be electrolyzed. Then, during the time course of an experiment:

$$2H_2O\,(l) \rightarrow 2H_2\,(g) + O_2\,(g) \tag{10}$$

thus, affecting the solution pH (therefore also affecting the EDL that forms on surface/liquid interfaces of particles, electrodes, and microfluidic channel walls). Electrolysis can be

avoided by operating in AC conditions with frequencies above a few kHz [30].

2.1.5 Joule heating

To describe Joule heating, consider a microfluidic channel filled with a liquid with conductivity σ_m subjected to an electric field **E**. In such a scenario, an electric current $I = \int \mathbf{J} \cdot \mathbf{dS}$ will develop (with **J** representing the current density). Joule heating is an electrothermal effect that takes place while an electric current I is flowing through a material [27]. This phenomenon is modeled by an electromagnetic heat source term (Fourier's Law), $Q_e = \mathbf{J} \cdot \mathbf{E}$, which is included in the heat equation—as a volumetric power source term—to calculate the temperature field, T.

$$\rho C_p \left(\frac{\partial T}{\partial t} + (\mathbf{v} \cdot \nabla T) \right) = \nabla \cdot (k \nabla T) + Q_e \tag{11}$$

where ρ is the density of the material, k is its thermal conductivity, C_p is its specific heat capacity, t is time, and **v** is the vector velocity field in the liquid domain.

In the present case, the material is the liquid, and many applications for iEK devices (e.g., manipulation of mammalian cells or proteins) require particles to be suspended in highly electrically-conductive solutions (producing larger values of I). Thus, incurring in significant heating that may damage the viability of the biological sample of interest [31]. Furthermore, the mechanical and electrical properties of the fluid and the particles suspended therein are temperature dependent. Therefore, the presence of Joule heating might significantly deviate the experimental observation from the expected outcome.

2.2 Fabrication

The fabrication processes used to produce iEK devices are just as important to this research field as the fundamentals described in subsection 2.1. This section does not attempt to provide a comprehensive treatise of all fabrication tools and protocols available to build iEK devices. Rather, it describes the generalities of the most widely used processes, so the non-expert reader may easily follow the upcoming sections. Excellent reviews and books have been published on this specific topic. The reader is therefore referred to [11,14,32] for details.

2.2.1 Photolithography

The goal of photolithography is to accurately transfer a pattern onto a photosensitive material [33]. Several photosensitive materials are commercially available. However, for iEK devices, most research groups use SU-8, a high contrast, epoxy-based negative photoresist. Therefore, the process described next can be used on negative photoresists only (see Fig. 2).

The photolithography process starts with a spin coating step to spread the material evenly on top of a flat surface (Figs. 2A and 2B). Depending on the spinning parameters (velocity, acceleration, and time) and the viscosity of the photoresist, the final photoresist layer thickness can be adjusted. Next, soft baking must be carried out. During this part of the process, the photoresist coated substrate is placed in a convection oven or on a hot plate to evaporate solvents and improve the substrate/photoresist adhesion (Fig. 2C). Temperature and time settings depend on the photoresist used and the thickness of the coated layer. Then, the photoresist material must be exposed to UV light through a photomask containing the pattern to transfer—transparent for the regions to keep, dark for the regions to remove (Fig. 2D). The exposed (and subsequently cross-linked) portions of the film are rendered insoluble to liquid developers. A post exposure bake is advised to complete the cross-linking process initiated by the UV exposure step (Fig. 2E). Finally, the photoresist coated substrate is immersed in a developer solution to dissolve the unexposed (unwanted) regions of the photoresist film (Fig. 2F). The recommended process settings for each step, as functions of photoresist layer thickness, are provided by the photoresist manufacturer.

The photolithography process is mostly used in the fabrication of molds or "masters" (the negative of the desired microfluidic device) of iEK devices. If a positive photoresist must be patterned via photolithography, one part of the process must change. For positive photoresists, the photomask will be transparent for the regions to remove and dark for the regions to keep.

2.2.2 Soft lithography

With soft lithography, the actual microfluidic channel is obtained based on the 'master' obtained via photolithography. For this process, the most popular material to use is PDMS. To start, the monomers must be mixed with a curing agent (10:1 ratio is generally used) and the mixture degassed in a vacuum chamber. Then, the degassed mixture is poured over the mold and heated (120°C for 15 minutes is a standard recipe) to solidify it (Figs. 2G and 2H). After this, PDMS can be carefully peeled off the mold (Fig. 2I) and bonded through plasma treatment on its substrate—generally, a PDMS-covered glass slide (Figs. 2J–2M) [34].

2.2.3 CNC milling and xurography

An altogether different approach to Photolithography + Soft Lithography for fabricating an insulator-based microfluidic device is that of Computer Numerical Control (CNC) milling [35]. With this process, the desired geometry is programmed in a computer through a specialized software and an automated mill, controlled by the computer, etches the microfluidic channel in a substrate. Materials such as glass and polymethyl methacrylate (PMMA) are commonly used for microfluidic applications. Also, Xurography represents

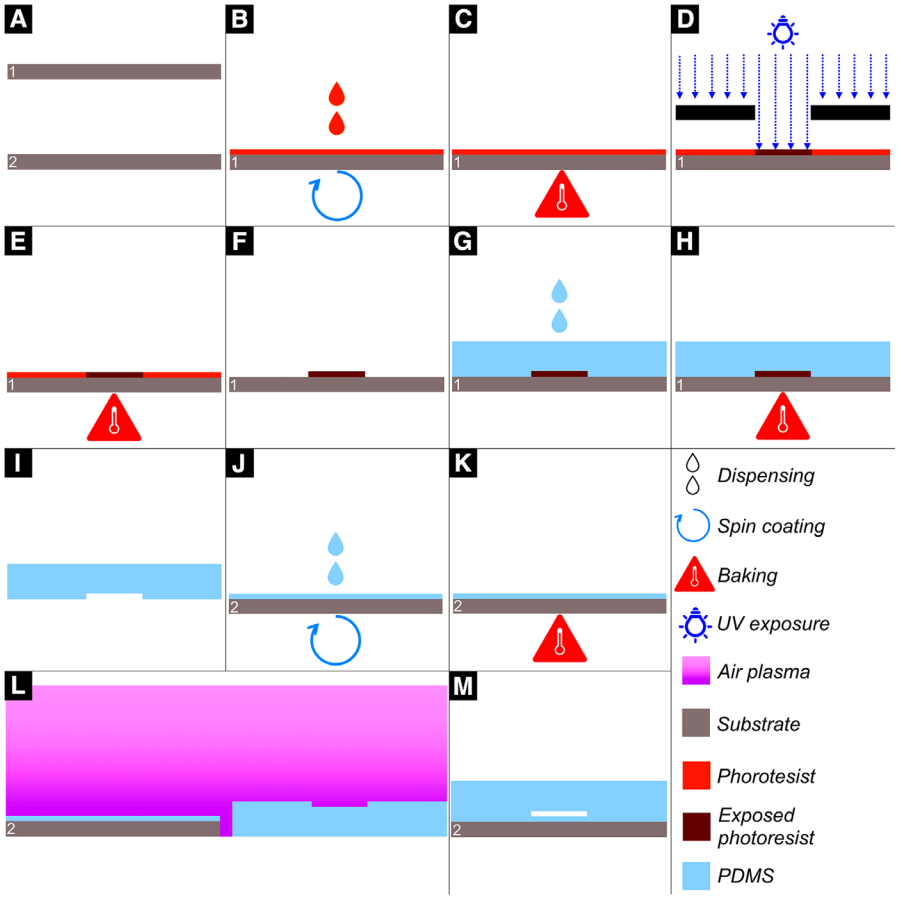

Figure 2. Schematic diagram of the fabrication process of a PDMS-based microfluidic device. **(B-F)** Photolithography. **(G-I)** Soft lithography. **(A)** Clean substrates for mold (1) and microfluidic channel (2). **(B)** Photoresist dispensing and spin coating. **(C)** Soft baking. **(D)** UV exposure through photomask. **(E)** Post exposure bake. **(F)** Development. **(G)** PDMS dispensing over mold. **(H)** PDMS curing. **(I)** PDMS peel off from mold. **(J)** PDMS dispensing and spin coating over substrate (2). **(K)** PDMS curing. **(L)** Air-plasma treatment. **(M)** Bonding.

an attractive alternative for simple microfluidic channel geometries (e.g., microfluidic channels featuring no structures within). The process is the same as in CNC milling, except for the tool and material to use, which in this case are a cutter (i.e., a plotter with a blade instead of a printing head), a Pressure Sensitive Adhesive (PSA) film, polycarbonate (PC), and a roller press [36].

2.2.4 Other techniques

Depending on the application at hand, other fabrication processes can be exploited to our benefit. If very high resolution is needed for the "master" (i.e., dimensions smaller than a few micrometers), electron beam (e-beam) lithography [37] or ion beam lithography [38] can be used. If larger dimensions are needed, 3D printing might be an attractive alternative to fabricate molds or the microfluidic channel itself [39]. Because these techniques are not frequently used in iEK devices, the interested reader is referred to [32,40] for details.

3 Insulator-based dielectrophoresis (iDEP)

Inspired by the abundant existing literature on eDEP, in 2003, Cummings and Singh used electrically-insulating posts built within a long microfluidic device to distort, what otherwise would be, a fairly uniform electric field distribution [16]. The electric field, $\mathbf{E}$, (with magnitude $|\mathbf{E}| = 800$ V/cm in the regions without insulating posts) was generated through the application of a large DC electric potential difference between two platinum electrodes, one immersed in the inlet reservoir of the channel and the other in the outlet reservoir. It is a fact that this design effectively produced regions of high and low electric field intensity—therefore $\nabla(\mathbf{E}_{RMS} \cdot \mathbf{E}_{RMS}) \neq 0$ in Eq. (1)—allowing for DEP to act upon polarizable particles (200 nm carboxylated latex nanospheres) suspended in a liquid contained therein. It is also a fact that these suspended particles featured a surface charge, which produced EP in the presence of $\mathbf{E}$. Finally, a third fact is the presence of ions in solution, which formed an EDL at the surface/liquid interface that interacted with $\mathbf{E}$ generating EO flow from the inlet to the outlet. Because the microfluidic channel did not contain posts everywhere, regions existed therein where the distribution of $\mathbf{E}$ remained mostly uniform (i.e., before and after the array of posts) and $\nabla(\mathbf{E}_{RMS} \cdot \mathbf{E}_{RMS}) \cong 0$. At these regions, it was observed that particles migrated with the fluid from the inlet to the outlet. Therefore, it was clear that electroosmosis dominated over electrophoresis, and that DEP was negligible there. Moreover, at the region of posts—where the electric field magnitude is amplified—particles

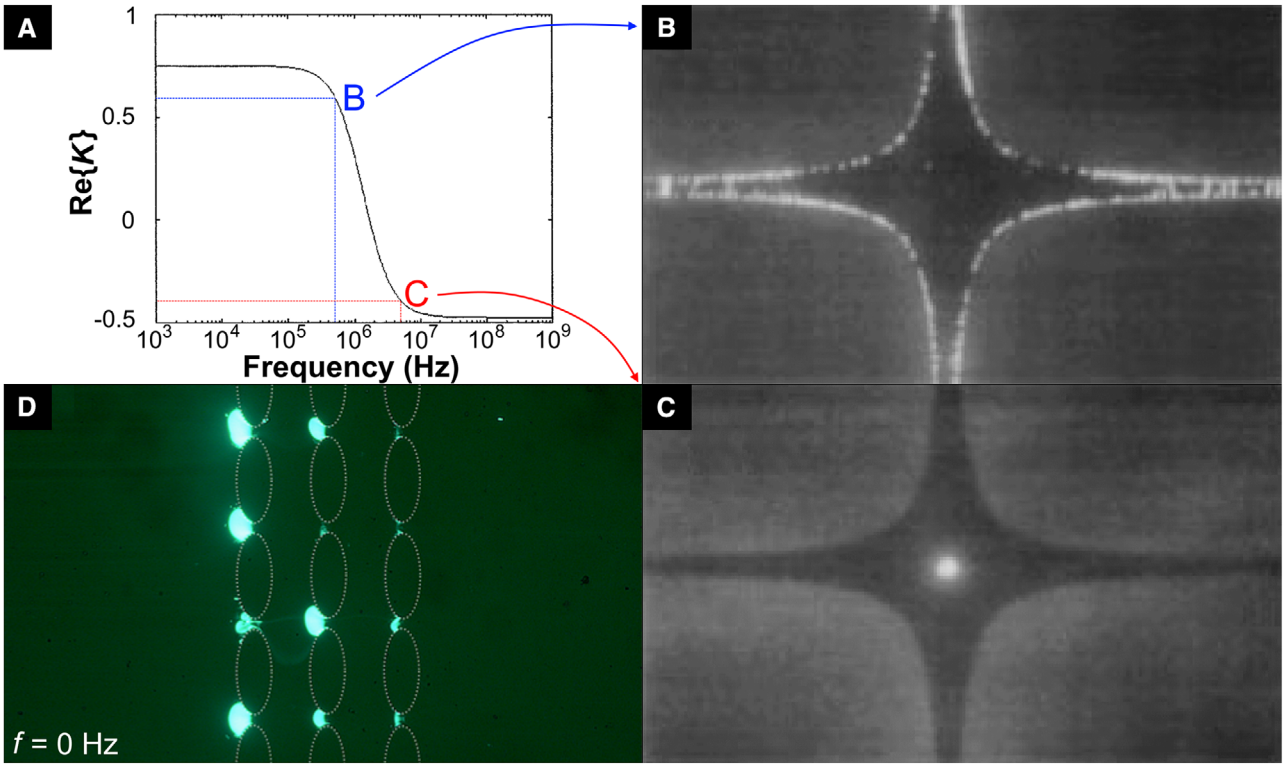

Figure 3. Comparison of eDEP and iDEP systems for manipulation of polystyrene spheres. **(A)** Theoretical plot of the real part of the Clausius–Mossotti factor of a polystyrene sphere as a function of frequency of the applied field (Reprinted with permission from [47], © (1999) American Chemical Society). **(B)** Example of experimental observation of pDEP at low frequencies in an eDEP system; in good agreement with the theoretical plot (Reprinted with permission from [47], © (1999) American Chemical Society). **(C)** Example of experimental observation of nDEP at high frequencies in an eDEP system; in good agreement with the theoretical plot (Reprinted with permission from [47], © (1999) American Chemical Society). **(D)** Example of experimental observation of particle repulsion—attributed to nDEP—from the regions between adjacent posts in a DC-iDEP system; not in agreement with the theoretical plot (Reprinted with permission from [48], © (2018) American Chemical Society).

kept on traveling from inlet to outlet at low applied voltages. Nonetheless, also at this region, if the applied voltage was increased sufficiently, there was a value for it that allowed particles to stop flowing ($|\mathbf{E}| = 1000$ V/cm in the region without posts). Because this experimental fact always took place at the regions where $\nabla(\mathbf{E}_{RMS} \cdot \mathbf{E}_{RMS}) \neq 0$ (i.e., slightly before each column of posts, at the gap between two posts in the same column), it was evident that an additional force was pushing the particles backwards, toward the inlet. This effect was attributed to nDEP. At this point, the insulator-based dielectrophoresis (iDEP) and the DC-iDEP terms were born.

For a while, iDEP devices like the one introduced in 2003 have allowed for successfully manipulating a wide range of particles, including bacteria [41], yeast [42], DNA [43], proteins [44], microalgae [45], and exosomes [46], among others. Interestingly, all these particles exhibited what would be considered nDEP (when stimulated with a DC voltage) for all tested scenarios. At this point we must pause and look at the theory of DEP and the reported observations obtained from eDEP experiments with polystyrene spheres (the standard particle of choice to characterize DEP systems) [47]. Theoretically, the Clausius–Mossotti factor defined in Eqn. (2) indicates that conductivities control polarization effects at DC and low frequencies and that, in contrast, permittivities take over at high frequencies. This implies that for a system where, for example, $\sigma_p > \sigma_m$ and $\varepsilon_p < \varepsilon_m$, the particle will experience pDEP at DC and low frequencies, nDEP at high frequencies, and a single crossover at some intermediate frequency as illustrated in Fig. 3A. Ermolina and Morgan extensively characterized suspensions of polystyrene spheres over a wide range of solution conductivities and found that, for most cases, pDEP would be observed at low frequencies and nDEP at high frequencies [28]. Fig. 3B and Fig. 3C reproduce micrographs of clear experimental evidence of pDEP and nDEP, respectively, in eDEP systems. Nonetheless, when a suspension of particles with properties similar to those reported for eDEP systems is analyzed in a DC-iDEP system, the observation indicates a repulsion of particles from regions with high $\nabla(\mathbf{E}_{RMS} \cdot \mathbf{E}_{RMS})$ (i.e., nDEP), not an attraction (i.e., pDEP) [48]. Such a scenario is shown in Fig. 3D. It is important to note that the plot shown in Fig. 3A does not include low frequencies and DC. However, Eqn. (2) and Eqn. (3) cannot provide an explanation for a possible second crossover frequency and nDEP at DC (nonetheless, a debate exists in the literature regarding the validity of the Maxwell-Wagner polarization model at low

frequencies [49]). Thus, some DC-iDEP studies opted for assuming $\sigma_p \sim 0$ to justify nDEP, with the added consequence of setting Re $\{K\} = -0.5$ (i.e., the strongest nDEP force for a given particle and $\nabla(\mathbf{E}_{RMS} \cdot \mathbf{E}_{RMS})$) [50,51]. It is evident that bioparticles are significantly more complex than polystyrene spheres and that more than one crossover frequency can be expected over a frequency sweep [52]. However, again, eDEP systems have successfully demonstrated pDEP at low frequencies [53], while DC-iDEP systems have not.

Following the assumption of $\sigma_p < \sigma_m$, to prove the applicability of the DEP theory to DC-iDEP devices, many papers were published where the electric field distribution present within the microfluidic channels was studied through computational modelling [54–57]. Finite Element Analysis (FEA) has been extensively used to model microchannel geometries varying in size and shape, also considering the size and shape of the posts. Results correctly indicate that there are regions in the devices where the magnitude of $\nabla(\mathbf{E}_{RMS} \cdot \mathbf{E}_{RMS})$ is similar to those obtained in eDEP designs [58]. Models evolved to further predict the combination of experimental parameters that would lead to particle trapping in these devices. At this point, the trapping condition (TC) was defined as the ratio of the DEP velocity to the EK velocity [59]:

$$TC = \frac{\mathbf{v}_{DEP} \cdot \mathbf{v}_{EK}}{\mathbf{v}_{EK} \cdot \mathbf{v}_{EK}} = \frac{\mu_{DEP} \nabla (\mathbf{E}_{RMS} \cdot \mathbf{E}_{RMS})}{\mu_{EK} |\mathbf{E}|^2} \cdot \mathbf{E} > 1 \qquad (12)$$

where $\mathbf{v}_{EK} = \mathbf{v}_{EP} + \mathbf{v}_{EO}$, and $\mu_{EK} = \mu_{EO} + \mu_{EP}$. Eq. (12) states that particle trapping will take place in regions where DEP dominates EO and EP. However, it was soon demonstrated that this ratio was unable to predict trapping unless it was multiplied by an empirical correction factor, c [42]. The use of this correction factor became widespread with values as high as 600 for some applications, as has been recently reviewed [60]. It must be noted that the requirement of an empirically-determined correction factor eliminates the possibility of predicting the outcome of any experiment performed in a DC-iDEP system.

At this point in our discussion, there are two clear questions to address 1) Why is it that no pDEP can be observed in DC-iDEP devices? and 2) What is represented by the correction factor c? Nonetheless, chronologically, while a quest for the answers to these questions (which will be presented in Section 4) was conducted, new knowledge that allowed improving the performance of DC-iDEP devices was developed. The Lapizco-Encinas group presented a parametric study to optimize the size and shape of insulating posts as well as the gap between themselves for maximizing $|\nabla(\mathbf{E}_{RMS} \cdot \mathbf{E}_{RMS})|$ [61]. Six geometries for the posts cross-section were thoroughly analyzed in that contribution (one circular, two oval, three rhombus-shaped with curved corners). It was demonstrated that slim oval posts with small gaps represent the best possible choice to reduce stimulation voltage and achieve particle trapping in DC-iDEP devices. Later, Perez-Gonzalez et al. proposed to model DC-iDEP systems as an electric circuit composed of a battery and resistors connected in series [48]. One of those resistors accounts for the resistivity of the suspending solution, while each additional resistor accounts for one column of posts. Therefore, an array containing N columns of posts acts as a voltage divider, reducing the voltage drop (and thus, the magnitude of the electric field) across each column as N increases. By removing columns of posts from a conventional array, a significant reduction of stimulation voltage was achieved to trap polystyrene particles. At the time, an important concern regarding this optimization emerged. If the magnitude of $\nabla(\mathbf{E}_{RMS} \cdot \mathbf{E}_{RMS})$ is being maximized, will the device incur in significant Joule Heating? Two different approaches were proposed in the literature to measure fluid temperature. In the first one, Rhodamine B was used by Nakano et al. as a temperature indicator (Rhodamine B fluorescence changes as a function of temperature) [62]. In the second one, Gallo-Villanueva et al. designed a serpentine-shaped metallic structure that, when placed in contact with the microfluidic channel, acted as a temperature sensor (the conductor resistivity changes as a function of temperature) [27]. It was demonstrated that the temperature rise for a wide range of experimental setups in DC-iDEP devices is almost negligible for several post geometries tested. This negligible temperature rise is mostly attributed to EOF injecting fresh solution continuously during an experiment.

AC voltages have also been used in iDEP devices. The Swami research group and the Ros research group have particularly exploited this approach to manipulate and characterize a wide range of bioparticles [63–69]. For this purpose, they use sophisticated electronic instrumentation to provide an AC voltage with sufficient amplitude to induce a detectable DEP response. Once more, we must pause and analyze the differences that exist between DC-iDEP systems and AC-iDEP systems. In DC-iDEP, because the electric field is not time dependent, EP and EOF play an important role in particle migration. In contrast, the electric field is time dependent in AC, changing its direction constantly during the time course of an experiment. This oscillation produces zero-average EP and EOF velocities [1]. Therefore, the only phenomenon to be considered in this scenario is, in fact, DEP. Actually, because of the zero-average EOF in AC-iDEP systems, it has been demonstrated that the rise in solution temperature is more significant than in DC-iDEP systems [27,70]. Despite this issue, cells, organelles, DNA, and proteins, have been successfully manipulated by DEP with AC fields. As expected, particles manipulated with AC-iDEP systems can exhibit both pDEP and nDEP responses.

Over the years, many variants have emerged from the original iDEP concept (see Fig. 4A). The Hayes group introduced "gradient-induced iDEP" where, by the inclusion of two identical arrays of posts in the lateral walls of a long rectangular channel (stimulated by a DC voltage), its cross-sectional area is gradually reduced [71]. These posts generally feature a triangular shape with one vertex pointing into the channel. Because the gap between posts becomes smaller as the particle of interest moves through the channel, at some point it will find a constriction that promotes the equilibrium between EP, EOF, and DEP [20]. This approach is very similar to the original concept of iDEP, as demonstrated by multi-section DC-iDEP systems used to separate particles from a

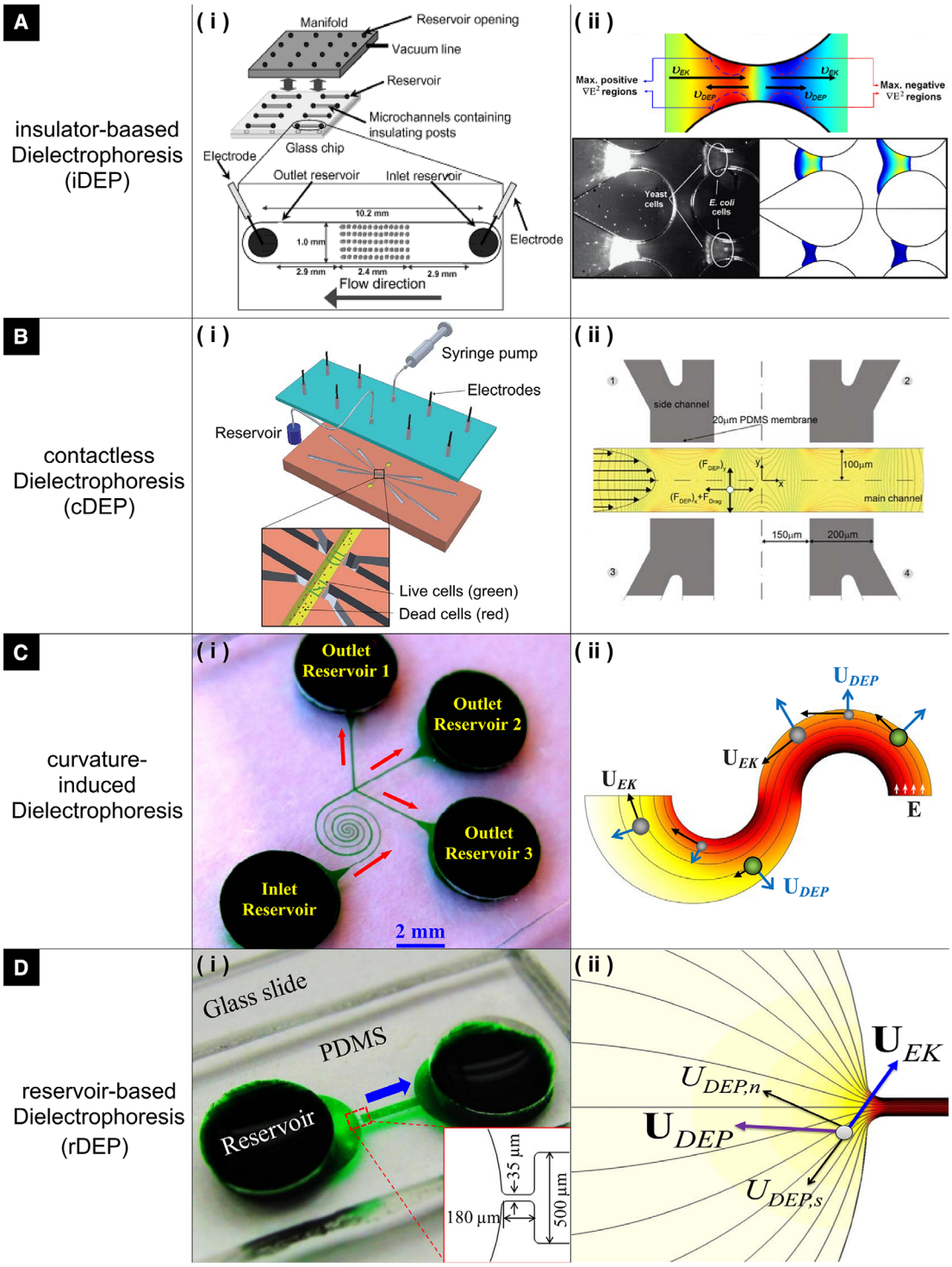

Figure 4. Comparison of different dielectrophoretic systems implemented in channels made from insulating materials that distort the distribution of electric field therein. **(i)** Schematic diagrams or photographs of devices. **(ii)** Physical description of the particle manipulation problem. **(A)** Insulator-based dielectrophoresis; microfluidic channels containing insulating obstacles that decrease the effective cross-sectional area of the device in specific regions (**i** Reprinted with permission from [17], © (2004) John Wiley and Sons, **ii** Reprinted with permission from [42], © (2011) John Wiley and Sons). **(B)** Contactless dielectrophoresis; microfluidic channels—that may or may not contain insulating obstacles—that are capacitively-coupled to lateral microchannels serving as external electrodes (Reprinted with permission from [79], © (2010) The Royal Society of Chemistry). **(C)** Curvature-induced dielectrophoresis; microfluidic channels with curvatures in its geometry preventing a uniform electric field distribution therein (Reprinted with permission from [21], © (2011) American Institute of Physics). **(D)** Reservoir-based dielectrophoresis; microfluidic channels that feature a very slim and thin constriction at its connection with a reservoir (Reprinted with permission from [22], © (2012) American Institute of Physics).

heterogeneous mixture. In these devices, each section features a different array of posts (i.e., differing in size, shape, or interpost gap) [56]. The gradient-induced iDEP concept has been successfully used to manipulate bacteria [72], viruses [73], and proteins [74]; while the multisection DC-iDEP concept has been recently able to separate a heterogeneous mixture of exosomes [46].

With a quite innovative approach, the Davalos research group developed "contactless DEP" (cDEP) [19]. In cDEP systems (see Fig. 4B) there are different channels serving different purposes. There is one main channel, where the bioparticles to manipulate must flow through, either by using a syringe pump or inducing a net DC-driven EOF [75]. In addition, there are two or more lateral channels filled with a highly conductive solution. Lateral channels are separated from the main channel by a thin insulating membrane. The external AC voltage is applied not across the main channel, but across the lateral channels, therefore avoiding electrolysis in the main channel. Each lateral channel is capacitively coupled to the main channel (the insulating membrane separating the lateral and main channels is the dielectric in the capacitor), therefore, a nonuniform AC electric field is induced within the main channel. Moreover, the main channel may or may not feature an additional post array to further distort the spatial distribution of the electric field. Contactless DEP systems are perhaps the only variant of the iDEP concept that has been proven to efficiently manipulate mammalian cells [76,77]. In addition, cDEP systems have also been used to manipulate bacteria and inert microparticles [78].

Following a different path, the Xuan group introduced two different variations of the original iDEP concept, "curvature-induced DEP" [21] and "reservoir-based DEP" (rDEP) [22]. In curvature-induced DEP (shown in Fig. 4C), a long channel is built (similar to iDEP and gradient-induced iDEP). However, in curvature-induced DEP, the channel features a spiral shape. The curvatures in the microfluidic channel distort the spatial distribution of an electric field generated between its ends [80]. This produces regions where the density of electric field lines changes abruptly (i.e., the innermost part of the curvature) and regions where the density of electric field lines changes slowly (i.e., the outermost part of the curvature) [81]. Particle manipulation in curvature-induced DEP channels has been mostly explored in the DC regime, where the successful manipulation of yeast cells has been demonstrated [82]. Finally, rDEP (see Fig. 4D) consists of a straight rectangular channel with inlet and outlet reservoirs. Nonetheless, the main feature of these systems can be found in a tiny region interconnecting the inlet reservoir with the main channel. There, a short rectangular microchannel—featuring a much smaller cross-section than that of the main channel—acts as a bridge to connect the reservoir with the main channel. This constriction produces a very large $|\nabla(\mathbf{E}_{RMS} \cdot \mathbf{E}_{RMS})|$ [83]. Successful separations of live and dead yeast cells, bacteria, and polystyrene spheres have been demonstrated in AC stimulated rDEP systems [22,84]. Moreover, the Buie group introduced 3DiDEP systems, where the tiny constriction is not found interconnecting any reservoir and the main channel (as in rDEP), but it resides within the main channel [85]. 3DiDEP channels are built through CNC milling processes on PMMA and have been shown to significantly reduce the voltage stimulation requirements to manipulate bioparticles [86,87].

The manipulation of bioparticles in iDEP devices (and its variants) has been thoroughly explored in the literature. Experimental observations of particle trapping are available for mammalian cells, bacteria, yeast, exosomes, DNA, proteins, and virus, among other bioparticles of interest as detailed in Table 1 and Table 2 for DC- and AC- driven systems, respectively. The interpretation of such observations is based in Eqns. (1), (2), and (4) for DEP of particles with spherical symmetry (and in modified versions of those equations for different particle geometries). However, a new theory of DEP has been recently proposed for polar bioparticles that states that the DEP force (pDEP in particular) experienced by this type of particles may be 3 or 4 orders of magnitude larger than those predicted by the classic DEP theory [24]. Recently, the Hayes group reported protein trapping in gradient-induced iDEP systems and explained their observations in terms of this theory [74].

4 Insulator-based electrokinetics (iEK)

As stated in section 3, there are two main questions to address in this review. The first one is: "Why is it that no pDEP can be observed in DC-iDEP systems?" The second one is: "What is represented by the correction factor c that is required in the DEP trapping condition?" I will provide plausible answers to these two questions in this section.

To start our discussion, consider a charged dielectric particle immersed in solution. The particle has radius a, and surface charge density ρ_q. The solution is an infinite symmetric electrolyte with valency $\pm Z$, ionic diffusivities D_+ and D_-, electrical conductivity σ_m, equilibrium concentration n_0, permittivity ε_m, viscosity η, and at temperature T. Extensive theoretical work has been carried out to explain what would happen to that charged particle when immersed in that solution and subjected to a high electric field [98–103]. This research field is known as "nonlinear electrophoresis", "electrophoresis of the second kind", or "induced-charge electrophoresis". As one of its name suggests, in this regime, electrophoresis will no longer be linearly dependent on the electric field. Instead, its relation will be nonlinear.

Induced-charge electrophoresis might be better explained through Fig. 5A, where two different scenarios are shown. In the first scenario (top), a negatively charged spherical particle is suspended in an ionic solution and no external field is present, $|\mathbf{E}| = 0$. An EDL forms around the particle to mirror its surface charge, which exhibits a potential—relative to the liquid bulk—in the order of the thermal voltage [$\varphi_T = k_B T/Ze = 25.85$ mV at room temperature ($T = 300$ K), with k_B representing the Boltzmann constant, and e representing the elementary charge]. The

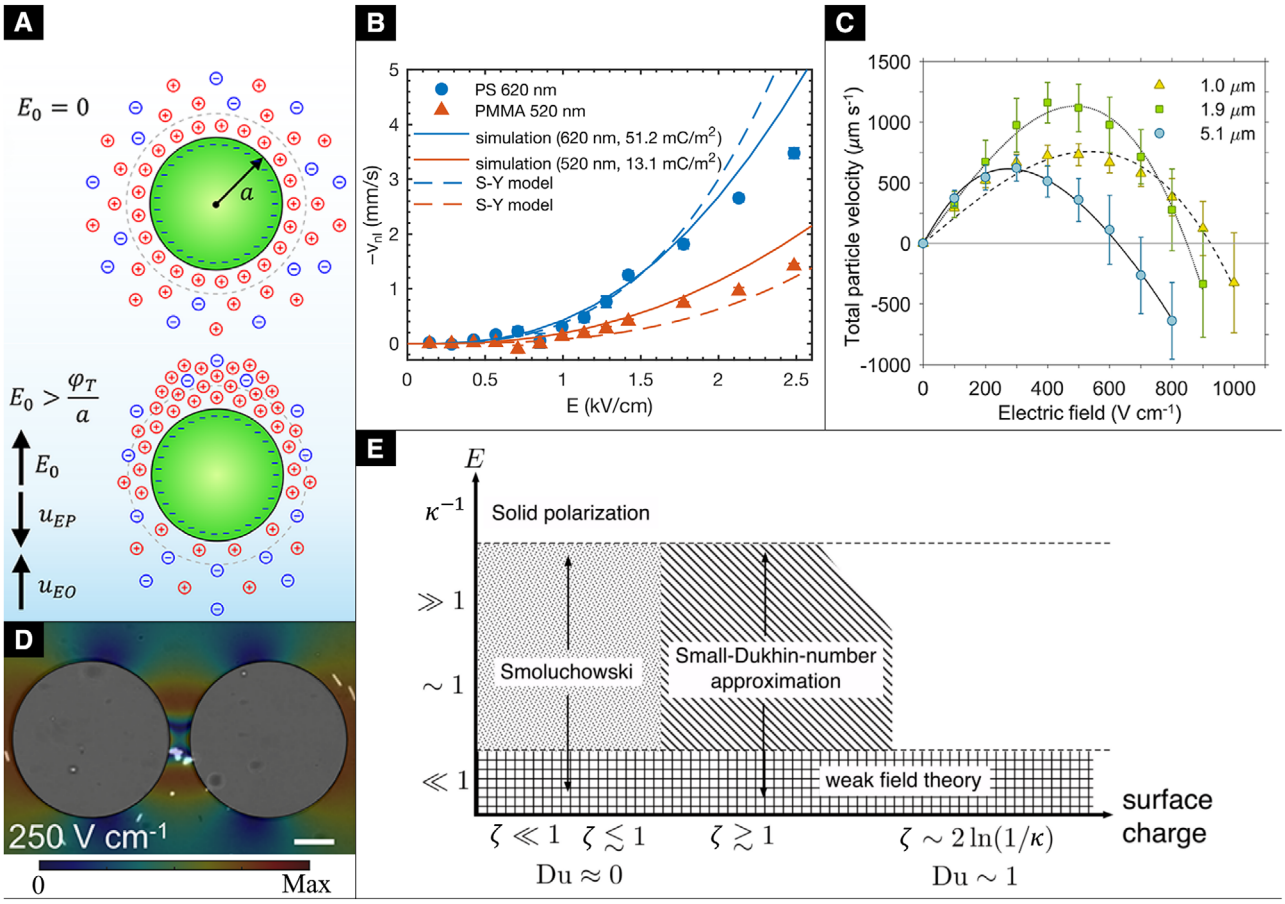

Figure 5. Nonlinear EP effects in microfluidics. **(A)** The electrical double layer surrounding a charged particle suspended in solution in the absence of an external electric field (top) and when the magnitude of the external electric field is larger than φ_T/a (bottom) (Reprinted with permission from [23], © (2020) American Chemical Society). **(B)** Experimental measurement, numerical modelling prediction, and analytical model prediction of the nonlinear electrophoretic velocity of two different charged particles as a function of applied electric field in a microfluidic channel with constant cross-section (Reprinted with permission from [110], © (2019) American Physical Society). **(C)** Experimental measurement of total particle velocity (i.e., linear electrophoretic velocity + linear electroosmotic velocity + nonlinear electrophoretic velocity) for three different particles as a function of applied electric field in a microfluidic channel with constant cross-section (Reprinted with permission from [23], © (2020) American Chemical Society). **(D)** Superposition of computational model prediction of particle velocity (colored surface plot) and experimental observation of particle trapping (white particles) in a DC-iEK microfluidic device with posts (gray circles) (Reprinted with permission from [23], © (2020) American Chemical Society). **(E)** The different regimes currently available to explain electric double layer formation as a function of Dukhin number and Debye length (Reprinted with permission from [108], © (2014) American Institute of Physics).

EDL—with a Debye length $\kappa^{-1} = \sqrt{\varepsilon_m \varphi_T / 2Zen_0}$ —exhibits and a Stern layer composed of positive counter ions and a diffuse layer that is mostly heterogeneous and uniform. In contrast, when an externally generated electric field with magnitude $|\mathbf{E}| > \beta = \varphi_T / a$ is present (β is the characteristic field strength), the EDL surrounding the particle develops a concentration polarization in its diffuse layer. This means that a surface charge over-screening exists in some region of the particle and an under-screening exists in the opposite region. In this case, the "deformed" diffuse layer of the EDL deviates from electroneutrality, altering the distribution of the applied electric field and giving rise to nonlinear electrokinetic phenomena [23,104].

In insulator-based DC electrokinetically-driven microfluidic devices, the electroosmotic velocity is generally obtained either through current monitoring [105] or through particle image velocimetry (PIV) of uncharged conducting microparticles, which are suspended in the solution to be used in the "DC-iDEP" experiment but contained in a long unobstructed rectangular channel [106,107]. Therefore, knowing v_{EO}, the permittivity of the solution ε_m, and the viscosity of the solution η, the wall zeta-potential ζ_w can be calculated from Eqns. (6) and (7). After this is carried out, the particle of interest is suspended in the solution and injected in the same long unobstructed rectangular channel. PIV is carried out again at low stimulation voltages and $\mathbf{v}_{EK} = \mathbf{v}_{EP} + \mathbf{v}_{EO}$ is measured. However, since $\mathbf{v}_{EO}$ is already known, $\mathbf{v}_{EP}$ can be easily calculated and ζ_p obtained from Eqns. (8) and (9). The problem with this approach is that the electric field generated within the microfluidic device during PIV is smaller than

φ_T/a. Therefore, linearity of EP and EOF with the electric field is guaranteed. However, insulating posts commonly used in DC-iDEP devices concentrate electric field lines in the inter-post gap region, significantly rising its magnitude [48]. Moreover, the voltages applied during a "DC-iDEP" experiment commonly surpass those used during the EP and EOF characterization stage. This means that, when a particle suspended in solution flows through a gap region, it will be subjected to a $\nabla(\mathbf{E}_{RMS}\cdot\mathbf{E}_{RMS})\neq 0$, but more importantly, it will be subjected to an electric field with magnitude $|\mathbf{E}|>\varphi_T/a$. As a result, the particle will experience a nonlinear electrophoretic force and the particle velocity can be expressed as:

$$\mathbf{v}_p=\mathbf{v}_{EO}+\mathbf{v}_{EP_{linear}}+\mathbf{v}_{EP_{nonlinear}}+\mathbf{v}_{DEP} \tag{13}$$

where $|\mathbf{v}_{EP_{nonlinear}}|$ has been shown to vary as $\sim|\mathbf{E}|^3$ or as $\sim|\mathbf{E}|^{3/2}$, depending on the experimental conditions [108,109].

Introducing the dimensionless ionic drag coefficient $\alpha^{\pm}=\varepsilon_m\varphi_T^2/\eta D_{\pm}$,and assuming a stationary Stokes flow (Reynolds number $\ll 1$), a thin EDL ($\kappa a\gg 1$), and an electric field $\mathbf{E}=E_x\,\mathbf{a}_x$, it is possible to calculate $\mathbf{v}_{EP}=\mathbf{v}_{EP_{linear}}+\mathbf{v}_{EP_{nonlinear}}$ far from the highly charged particle surface via the weakly nonlinear version of the Schnitzer and Yariv model [109]

$$v_{EP}=\mu_{EP}^{(1)}E_x+\mu_{EP}^{(3)}E_x^3 \tag{14}$$

with mobilities

$$\mu_{EP}^{(1)}=-\frac{\varepsilon_m\varphi_T}{\eta}\left(\frac{\zeta_0+\mathrm{Du}\cdot\ln(16)}{1+2\mathrm{Du}}\right) \tag{15}$$

$$\mu_{EP}^{(3)}=-\frac{a^2\varepsilon_m}{\eta\varphi_T}f\left(\mathrm{Du},\zeta_0,\alpha,\acute{\alpha}\right) \tag{16}$$

In Eqns. (15) and (16), $\mathrm{Du}=(1+2\alpha^+)\,\rho_g/2Zen_0a$ is the modified Dukhin number, $\zeta_0=2\ln(\rho_q/\varepsilon_m\kappa\varphi_T)$ is the dimensionless particle zeta potential, $\alpha=(\alpha^++\alpha^-)/2$ and $\acute{\alpha}=(\alpha^+-\alpha^-)/2$ are two dimensionless coefficients related to the ionic drag, and $f(\mathrm{Du},\zeta_0,\alpha,\acute{\alpha})$ is a nonlinear function of the EK properties of the particle/liquid system defined as:

$$f\left(\mathrm{Du},\zeta_0,\alpha,\acute{\alpha}\right)=\frac{\mathrm{Du}\left(k_0+k_1\mathrm{Du}+k_2\mathrm{Du}^2+k_3\mathrm{Du}^3+k_4\mathrm{Du}^4+k_5\mathrm{Du}^5\right)}{840(1+2\mathrm{Du})^4\,(1+4\mathrm{Du})\,(1+6\mathrm{Du})} \tag{17}$$

The definitions for the k_i coefficients are shown in the original work by Schnitzer and Yariv [109]. Eqns. (14)–(17) are valid for cases where $(E_x/\beta)\sim\mathcal{O}(1)$. However, this condition is not always satisfied. An alternative model for the electrophoretic velocity exists for cases with arbitrary magnitude of E_x and small (but finite) Du.

$$v_{EP}=\frac{\varepsilon_m\varphi_T^2}{\eta a}\left(\zeta_0\frac{E_x}{\beta}+\mathrm{Du}\mathcal{U}_1\right) \tag{18}$$

where $\mathcal{U}_1$ is a nonlinear function that varies as $\sim(E_x/\beta)^{3/2}$ (see [108] for details).

Recently, the Keyser research group reported careful experimental observations of nonlinear electrophoretic velocity of polystyrene and PMMA particles in long unobstructed rectangular channels [110]. For this, they generated electric fields with magnitudes in excess of 1 kV/cm. In addition to the experimental observations, they conducted computational modelling of the electrokinetic behavior of the particles in their microfluidic device. Computational model predictions and experimental observations were in good agreement. Moreover, they also compared their experimental observations against the theoretical curves of nonlinear electrophoretic particle velocity—Eqns. (14) and (18)—proposed by Shnitzer and Yariv [108,109,111]. Theoretical predictions and experimental observations were also in good agreement. This is shown in Fig. 5B. Then, in 2020, Cardenas-Benitez et al. characterized total particle velocity—Eqn. (13)—in long unobstructed rectangular channels and in "DC-iDEP" channels featuring only two circular posts [23]. In the unobstructed channels it was observed that particle motion would have an average value of zero for a certain magnitude of the electric field $|\mathbf{E}|\neq 0$. This value would be different for different particles and, as a result, it was called the "electrokinetic equilibrium condition", E_{EEC} (Fig. 5C shows the E_{EEC} for three types of particles. It can be observed that when $|\mathbf{E}|<E_{EEC}$, electroosmosis dominates and particles move in the direction of fluid flow. It can also be observed that when $|\mathbf{E}|>E_{EEC}$, the combination of linear and nonlinear EP dominates, and particles move in the direction opposite to fluid flow). If $\mathbf{v}_{DEP}$ is neglected and $|\mathbf{v}_{EP_{nonlinear}}|\propto|\mathbf{E}|^3$ is assumed in Eqn. (13), then

$$E_{EEC}=\sqrt{-\frac{\mu_{EP}^{(1)}+\mu_{EO}}{\mu_{EP}^{(3)}}} \tag{19}$$

therefore, if E_{EEC}, $\mu_{EP}^{(1)}$, and μ_{EO} are measured experimentally, $\mu_{EP}^{(3)}$ can then be calculated. Moreover, they proposed that for a particle to be trapped in a region of a "DC-iDEP" microfluidic device, the electric field at that region must have a magnitude $|\mathbf{E}|=E_{EEC}$. This proposition was successfully validated experimentally. Also, computational modeling allowed predicting the conditions for particle trapping with no requirement of a correction factor. Prediction error was smaller than 10% for all studied cases (an example is shown in Fig. 5D, where a prediction from a computational model has been superimposed with an experimental observation). In addition, it was possible for them to derive an analytical expression for the electric field distribution in their channel, providing additional insight into the geometric variables controlling "electric field amplification" in the region between posts. Finally, this work demonstrated that the DEP force acting on those particles in those experiments is, for every practical purpose, negligible, and that, therefore, DC-iEK is a much better suited term to describe the technology than DC-iDEP is. Nonetheless, this work also demonstrated that a gap needs to be filled in the literature, for most DC-iEK experiments are performed in setups described by the blank region in Fig. 5E, for which no analytical models of nonlinear electrophoretic velocity

exist. The electrokinetic equilibrium condition, E_{EEC}, has been recently exploited primarily by the Lapizco-Encinas research group to prove that the electrokinetic equilibrium condition is, in fact, independent of the microfluidic channel design [112], and also to characterize the nonlinear EP mobility of different cells and protein aggregates [113–115].

Going back to our two questions, I can now provide those two plausible answers based on the recent findings discussed in the previous paragraphs. First, it can be concluded that it was impossible to observe pDEP in "DC-iDEP" channels because the DEP contribution to particle migration was practically negligible—several orders of magnitude smaller than EOF and EP. Second, it can also be concluded that the correction factor c used in the trapping condition in Eqn. (12) accounted for the unconsidered nonlinear EP effects. As a matter of fact, Eqn. (12) must be significantly altered, for the equilibrium that leads to particle trapping in these systems seems to be mostly dependent on EP and EOF. However, careful and extensive additional experimental work must be carried out to further validate these conclusions. Moreover, induced-charge electroosmosis (also known as electroosmosis of the second kind or nonlinear electroosmosis), has recently been shown to also play a significant role in DC-iEK systems. Strong evidence was presented by the Buie and Xuan research groups on its potential to produce particle recirculation (together with electrothermal flow produced by Joule heating) near trapping regions [70,116–120].

5 Future perspectives and concluding remarks

The future of this research field holds great potential for innovative contributions. From its conception and until recently, it was fully accepted that DEP was the dominant mechanism for particle manipulation in DC-iEK systems. It was acknowledged that EP and EOF were present in the system, but their role in particle migration was considered to be only secondary to DEP. Equipped with this theory, many research teams achieved extraordinary experimental observations (see Table 1 and Table 2) of the manipulation of a wide range of bioparticles; even a company (LabSmith) was created to provide the instrumentation required to conduct experimental work in this field and analyze the observations. It is therefore evident that electrokinetically-driven insulator-based microfluidic devices hold great value for many biomedical and biotechnological applications.

Two decades after this technology was born, a new possible interpretation of its experimental observations has risen from theories developed many years ago on nonlinear EK phenomena. In this interpretation, DEP is not presented as the main character of the story. This new perspective does not challenge the experimental observations previously reported, it merely concludes something different about the experiment. For example, let us consider a heterogeneous mixture of two types of particles (type A and type B)—of the same size but with different electrical properties—injected into a DC-iEK system. If, at a certain voltage, one of those two types of particles (e.g., type B) gets trapped while the other (type A) keeps flowing, the classic DC-iDEP theory would make a conclusion about the electrical conductivity of both types of particles with respect to that of the suspending solution (i.e., type A particles are more conductive than type B particles, and both types of particles are less conductive than the suspending solution). In contrast, the new perspective would make a conclusion regarding the surface charge density of both types of particles (i.e., the surface charge density of type B particles is greater than that of type A particles).

Despite all the attractive and intriguing features of DC-iEK systems, we must recognize that this technology presents limitations that have been successfully solved by using AC-based approaches. All contributions reviewed in Table 2 evidence that having the frequency of the applied voltage as an additional control parameter during a particle manipulation experiment, provides a new level of flexibility to the technology. The frequency of the applied voltage allows probing different polarization regimes in the bioparticles (i.e., the conductive regime at low frequencies and the dielectric regime at high frequencies). Moreover, from all distinct iDEP approaches, contactless DEP avoids the unwanted effects of electrolysis in the main channel, allowing for the bioparticles to remain in their most adequate environment through the experiment. Unfortunately, just as in any RC circuit, a cutoff frequency (controlled by the thickness and composition of the insulating membrane) exists in cDEP systems, eliminating the possibility to test the DEP effect on particles over a wide frequency range.

There are many challenges our research community must address in the years to come. The first challenge I can see is that of reducing the stimulation voltage requirements of all iEK devices (both DC-driven and AC-driven). Because our electrodes are relatively far away from each other (in comparison to distances found in eDEP devices) we normally require voltages superior to 100 V to achieve particle trapping. If working in DC, this requirement can be readily met by using a not so bulky power source. If working in AC, however, we need to connect our waveform generator to an RF amplifier, and sometimes we need an additional amplification step provided by a transformer. All this goes against the main objective of the technology, which is to produce portable LOC or POC devices. Efforts have been made towards reducing voltage requirements [121], but it is clear that much more work is still needed. A second challenge to address is the lack of an analytical model of the EDL that is valid in the blank region shown in Fig. 5E. It must be clear that Eqn. (19) only applies to scenarios where the nonlinear EP velocity varies as $\sim |\mathbf{E}|^3$. If $|\mathbf{v}_{EP_{nonlinear}}|$ exhibits any other dependency with the electric field, the E_{EEC} can be measured, but it will not allow us to extract information about the electrokinetic properties of the particle of interest in the way Eqn. (19) does. Finally, a critical challenge is to test the validity of the new theory that takes into consideration nonlinear electrokinetics in DC-driven devices. Up until today, it has been validated using a few different channel designs, some polystyrene spheres, a

Table 1. Direct-current insulator-based electrokinetic devices for bioparticle trapping

Target Particle (characteristic dimension)	E-field modifier description	σ_m (μS/cm)	pH	Voltage (V)	Application / Cause	Ref.
E.coli (2.38±0.32 μm long 0.96±0.21 μm wide), ***B. subtilis***, (4.86±0.41 μm long 1.94±0.19 μm wide) ***S. cerevisiae*** (3.15±0.2 μm radius)	Two designs of a 4 × 16 array of 3D insulating posts. One with rhombus-shaped cross-section, the other with circular cross-section. Both diagonals of each rhombus measure 200 μm. The diameter of each circle measures 200 μm. Posts are separated by 50 μm gaps (vertically and horizontally).	20, 30	8.0	300–1000	Particle trapping and assessment of viability / nDEP	[88]
DNA (5.3 kbp)	4 × 10 array of 3D insulating posts with circular cross-section. The diameter of each circle measures 470 μm. Posts are separated by 40 μm gaps (vertically and horizontally).	100–120	10.8–11.15	2000	Particle trapping / nDEP	[43]
S. capricornutum (∼5 μm "apparent" radius)	Two designs of a 4 × 8 array of 3D insulating posts with circular cross-section. The diameter of each circle in the first design measures 440 μm. Posts are separated by 80 μm gaps (vertically). The diameter of each circle in the second design measures 470 μm. Posts are separated by 40 μm gaps (vertically).	2.25 and 187.5	5.8 and 9.0	600–2500	Selective particle trapping and assessment of viability / nDEP	[45]
RNase A (20 kDa)	A 3 × 6 array of 3D insulating posts with rhombus-shape cross-section. Both diagonals of each rhombus measure 650 μm. Posts are separated by 10 μm gaps (vertically and horizontally). Rows 1 and 3 only feature half posts (triangles). Each triangle has one vertex pointing to its adjacent rhombus.	100	8.0	2500–4000	Particle trapping / nDEP	[31]
MCF-7 derived exosomes (102.01±3.5 nm radius)	Two designs of a 4 × 3 array of 3D insulating posts with oval-shaped cross-section. The major and minor axes of each oval measure 450 μm and 90 μm, respectively. Posts in the first design are separated by 15 μm gaps (vertically) and 50 μm gaps (horizontally). Posts in the second design are separated by 10 μm gaps (vertically) and 50 μm gaps (horizontally).	14	5.5	200–2000	Selective particle trapping and separation / nDEP	[46]
MCF-7 (15 μm radius) **MDA-MB-231** (15 μm radius) **PBMC** (2.8–7.5 μm radius)	Two 3D insulating posts with quasi-triangular cross section. The base and height of each triangle measure ∼60 μm and ∼40 μm, respectively. Triangles are facing each other and separated by 30 μm.	270	∼5.0	80	Selective particle trapping and separation / nDEP	[89]

(*Continued*)

Table 1. (Continued)

Target Particle (characteristic dimension)	E-field modifier description	σ_m (μS/cm)	pH	Voltage (V)	Application / Cause	Ref.
L. monocytogenes (0.25–2 μm radius 0.5–2 μm length)	An array of many triangular posts in the lateral walls of the microfluidic channel pointing into it. The gap between each pair of triangles decreases in size from 945 μm to 27 μm along the channel	300	7.4	0–500	Particle isolation / nDEP	[90]
Sindbis virus (34 nm radius)	An array of 24 triangular posts in each lateral wall of the microfluidic channel. Each triangle points into the channel. The gap between each pair of triangles decreases in size from 30 μm to 3 μm along the channel	2120	7.2	0–700	Particle trapping / nDEP	[73]
NSPCs (75 μm radius)	An array of 27 triangular posts in each lateral wall of the microfluidic channel. Each triangle points into the channel. The gap between each pair of triangles decreases in size from 73 μm to 25 μm along the channel	NA	7.6	90	Particle identification / nDEP	[91]
RBCs (3.1–4.1 μm radius 0.8–2.5 μm thickness) **MyO** (18 kDa) **H-FABP** (15 kDa)	An array of 24 triangular posts in each lateral wall of the microfluidic channel. Each triangle points into the channel. The gap between each pair of triangles decreases in size from 73 μm to 25 μm along the channel	NA	7.2–7.4	100–3000	Particle capture / nDEP	[92]
G. sulfurreducens (∼1.3 μm major semi axis ∼0.4 μm minor semi axis) ***S. oneidensis*** (NA) ***E. coli*** (NA)	A constriction (50 μm long, 50 μm wide, 50 μm deep) within an otherwise uniform cross-section microfluidic channel (1 cm long, 500 μm wide, 500 μm deep).	100	6.8	0–100	Particle characterization / pDEP	[86]
Polystyrene beads (5 μm radius) ***B. cereus*** (NA) ***E. coli*** (NA)	A constriction (50 μm long, 50 μm wide, 50 μm deep) within an otherwise uniform cross-section microfluidic channel (1 cm long, 500 μm wide, 500 μm deep).	100	7.0	10–100	Particle trapping / nDEP	[85]
P. aeruginosa (NA) ***S. mitis*** (NA)	A constriction (50 μm long, 50 μm wide, 50 μm deep) within an otherwise uniform cross-section microfluidic channel (1 cm long, 500 μm wide, 500 μm deep).	100	7.0	10–100	Particle characterization / nDEP	[87]
S. cerevisiae (3±1 μm radius)	Two spirals in opposite directions. Each spiral has four equally separated loops and measures 2.5 cm long in total. The diameter of the inner most semi-circle is 100 μm. The channel is everywhere 50 μm wide and 25 μm deep. The radial distance between adjacent loops is 150 μm	210	NA	0–300	Particle separation / nDEP	[82]

Table 2. Alternating-current insulator-based dielectrophoretic devices for bioparticle trapping (voltages marked with an * were not identified as V_p, V_{pp}, or V_{RMS} in the original work)

Target Particle (characteristic dimension)	E-field modifier description	$\varepsilon_{r,m}$	σ_m (μS/cm)	pH	V_p (V)	Frequency (Hz)	Application / Cause	Ref.
DNA (1.0, 10.2, 19.5, 48.5 kbp)	A constriction at the end of the buffer-filled channel followed by a division of the channel into five outlets. The insulating constrictions that separate the five outlets further distort the distribution of electric field.	NA	NA	7.7	50–1200	$50–20 \times 10^3$	Continuous particle separation / pDEP and nDEP	[67]
MCF10A (6.05±0.1 μm radius)	A couple of insulating structures reducing the cross-section of the microfluidic device. The end-shape of the design resembles a funnel.	80	700	NA	17	200×10^3 and 50×10^6	Single cell analysis / pDEP and nDEP	[93]
Mitochondria (75 nm–1 μm radius)	An array of insulating posts with rounded-corners-triangular cross-section within the microfluidic device. As a result of the presence of this array, regions of high and low concentration of electric field develop within the microfluidic channel.	NA	250–300	7.2–7.4	> 200	$0–50 \times 10^3$	Particle isolation / nDEP	[68]
S. cerevisiae (2.5–3.0 μm radius)	A 3.3 mm long straight microchannel with a 5 mm diameter reservoir at each end. The channel is 500 μm wide and has a constriction section of 35 μm width and 180 μm length at the entrance. The channel is uniformly 25 μm deep.	78	210	NA	> 141.42	$1 \times 10^3–500 \times 10^3$	Particle separation and assessment of viability / pDEP and nDEP	[22]
DNA origami (∼3.5 nm radius 380 nm length)	An array of 3D insulating posts with oval-shaped cross-section. The major and minor axes of each oval measure 11.6 μm and 10.5 μm, respectively. Posts in the first design are separated by 2.1 μm gaps (vertically and horizontally).	80	$1 \times 10^3–10 \times 10^3$	8.3	500–2100 *	$60–15 \times 10^3$	Particle trapping and manipulation / pDEP	[69]
S. cerevisiae (∼3.5 μm radius)	Two opposing identical arrays of 20 triangular ratches along the microchannel sidewalls. The peak-to-peak distance of two consecutive ratches is 250 μm. The widest part of the channel is 500 μm, while the narrowest part is 100 μm.	NA	200	NA	50–200	< 10	Particle focusing / nDEP	[94]
HEK (∼10 μm radius **MEF** (∼10 μm radius)	An array of insulating posts with rhombus-shaped cross-section within the microfluidic device. The direction of the applied electric field is perpendicular to that of the fluid velocity field.	NA	1.5×10^3	NA	5	$100 \times 10^3–45 \times 10^6$	Particle quantification / pDEP and nDEP	[65]

(*Continued*)

Table 2. (Continued)

Target Particle (characteristic dimension)	E-field modifier description	$\varepsilon_{r,m}$	σ_m (μS/cm)	pH	V_p (V)	Frequency (Hz)	Application / Cause	Ref.
E. coli (NA)	SU-8 membrane with a honeycomb patterned etched on it. The membrane is perpendicular to the flow direction (i.e., the vector normal to its surface is antiparallel to the flow velocity).	NA	2–5	NA	Up to 160 *	10×10^3–10×10^6	Particle concentration / pDEP	[95]
Streptavidin (∼5 nm radius)	Two triangular obstacles fabricated on the walls of the microfluidic channel. Triangles point at each other, reducing the cross-sectional area of the microfluidic device. The width of the channel decreases from 500 μm to 0.1 μm, 1 μm, and 10 μm.	NA	1×10^3–100×10^3	NA	150	$<1 \times 10^6$	Particle trapping / pDEP	[64]
E. coli (NA) ***S. aureus*** (NA)	An array of electrically insulating microposts embedded within the microfluidic channel	NA	8	NA	95	1×10^3–1×10^6	Selective particle trapping / pDEP and nDEP	[96]
Polystyrene beads (5, 7.5 μm radius) ***S. cerevisiae*** (NA)	Tapered constriction within the PDMS microfluidic device. The width of the channel decreases from 1000 μm to 60 μm.	NA	600	NA	635	5×10^3	Particle concentration / nDEP	[97]
THP-1 (7.7±1 μm radius)	Wavy lateral channels separated from the main channel by a thin insulating membrane. The main channel has a nonuniform cross-section because of the presence of the lateral channels. In addition to this, an array of posts with circular cross-section exists within the main channel to further deform the electric field distribution.	80	100	NA	28.28–212.13	200×10^3–500×10^3	Particle isolation / pDEP	[79]
MCF10A (9.25 μm radius) **MCF7** (9.1 μm radius) **MDA-MB-231** (8.93 μm radius)	Wavy lateral channels separated from the main channel by a thin insulating membrane. The main channel has a nonuniform cross-section because of the presence of the lateral channels. In addition to this, an array of posts with circular cross-section exists within the main channel to further deform the electric field distribution.	80	100	NA	28.28–70.71	150×10^3–350×10^3	Selective particle concentration / pDEP and nDEP	[77]

few bacteria, and a few protein aggregates. It would be dangerous to assume it is true for every possible scenario and that DEP can always be neglected. Much more experimental work is still needed to assess its completeness and applicability.

This work was financially supported by the Nano- Sensors & Devices Research Group (0020209I06) and the Federico Baur Endowed Chair in Nanotechnology (0020240I03) at Tecnologico de Monterrey. Braulio Cardenas-Benitez is acknowledged for broad discussions on nonlinear electrokinetics. Jose I. Gomez-Quinones is acknowledged for discussions on the artwork contained in this review.

The author has declared no conflict of interest.

Data availability statement

The data that support the findings of this study are available from the corresponding author upon reasonable request.

6 References

[1] Morgan, H., Green, N. G., *AC Electrokinetics: Colloids and Nanoparticles*, Research Studies Press, Philadelphia 2003.

[2] Kim, U., Shu, C.-W., Dane, K. Y., Daugherty, P. S., Wang, J. Y. J., Soh, H. T., *Proc. Natl. Acad. Sci. USA* 2007, *104*, 20708–20712.

[3] Hughes, M. P., Morgan, H., Rixon, F. J., Burt, J. P. H., Pethig, R., *Biochim. Biophys. Acta Gen. Subj.* 1998, *1425*, 119–126.

[4] Sanchis, A., Brown, A. P., Sancho, M., Martínez, G., Sebastián, J. L., Muñoz, S., Miranda, J. M., *Bioelectromagnetics* 2007, *28*, 393–401.

[5] Markx, G. H., Talary, M. S., Pethig, R., *J. Biotechnol.* 1994, *32*, 29–37.

[6] Deng, Y.-L., Chang, J.-S., Juang, Y.-J., *Bioresour. Technol.* 2013, *135*, 137–141.

[7] Martinez-Duarte, R., Camacho-Alanis, F., Renaud, P., Ros, A., *Electrophoresis* 2013, *34*, 1113–1122.

[8] Giraud, G., Pethig, R., Schulze, H., Henihan, G., Terry, J. G., Menachery, A., Ciani, I., Corrigan, D., Campbell, C. J., Mount, A. R., Ghazal, P., Walton, A. J., Crain, J., Bachmann, T. T., *Biomicrofluidics* 2011, *5*, 24116.

[9] Jones, T. B., Jones, T. B., *Electromechanics of Particles*, Cambridge University Press, Cambridge, New York 2005.

[10] Pohl, H. A., *J. Appl. Phys.* 1951, *22*, 869–871.

[11] Martinez-Duarte, R., *Electrophoresis* 2012, *33*, 3110–3132.

[12] Kirby, B. J., *Micro-and Nanoscale FluidMechanics: Transport in Microfluidic Devices*, Cambridge University Press, Cambridge, New York 2010.

[13] Elitas, M., Martinez-Duarte, R., Dhar, N., McKinney, J. D., Renaud, P., *Lab Chip* 2014, *14*, 1850–1857.

[14] Madou, M. J., *Fundamentals of Microfabrication: The Science of Miniaturization*, CRC Press, Boca Raton 2018.

[15] Park, S., Koklu, M., Beskok, A., *Anal. Chem.* 2009, *81*, 2303–2310.

[16] Cummings, E. B., Singh, A. K., *Anal. Chem.* 2003, *75*, 4724–4731.

[17] Lapizco-Encinas, B. H., Simmons, B. A., Cummings, E. B., Fintschenko, Y., *Electrophoresis* 2004, *25*, 1695–1704.

[18] Lapizco-Encinas, B. H., *Electrophoresis* 2019, *40*, 358–375.

[19] Shafiee, H., Caldwell, J. L., Sano, M. B., Davalos, R. V., *Biomed. Microdevices* 2009, *11*, 997.

[20] Jones, P. V, Hayes, M. A., *Electrophoresis* 2015, *36*, 1098–1106.

[21] Zhu, J., Xuan, X., *Biomicrofluidics* 2011, *5*, 24111.

[22] Patel, S., Showers, D., Vedantam, P., Tzeng, T.-R., Qian, S., Xuan, X., *Biomicrofluidics* 2012, *6*, 34102.

[23] Cardenas-Benitez, B., Jind, B., Gallo-Villanueva, R. C., Martinez-Chapa, S. O., Lapizco-Encinas, B. H., Perez-Gonzalez, V. H., *Anal. Chem.* 2020, *92*, 12871–12879.

[24] Seyedi, S. S., Matyushov, D. V, *J. Phys. Chem. B* 2018, *122*, 9119–9127.

[25] Chang, H.-C., Yeo, L. Y., *Electrokinetically-Driven Microfluidics and Nanofluidics*, Cambridge University Press, Cambridge, New York 2010.

[26] Erickson, D., Sinton, D., Li, D., *Lab Chip* 2003, *3*, 141–149.

[27] Gallo-Villanueva, R. C., Perez-Gonzalez, V. H., Cardenas-Benitez, B., Jind, B., Martinez-Chapa, S. O., Lapizco-Encinas, B. H., *Electrophoresis* 2019, *40*, 1408–1416.

[28] Ermolina, I., Morgan, H., *J. Colloid Interface Sci.* 2005, *285*, 419–428.

[29] Gagnon, Z. R., *Electrophoresis* 2011, *32*, 2466–2487.

[30] Glasstone, S., *An Introduction to Electrochemistry*, Read Books Ltd., Redditch, Worcestershire, UK 2011.

[31] Mata-Gomez, M. A., Perez-Gonzalez, V. H., Gallo-Villanueva, R. C., Gonzalez-Valdez, J., Rito-Palomares, M., Martinez-Chapa, S. O., *Biomicrofluidics* 2016, *10*, 33106.

[32] Gad-el-Hak, M., *The MEMS Handbook*, CRC press, Boca Raton 2001.

[33] Miyajima, H., Mehregany, M., *J. Microelectromechanical Syst.* 1995, *4*, 220–229.

[34] Xia, Y., Whitesides, G. M., *Annu. Rev. Mater. Sci.* 1998, *28*, 153–184.

[35] Guckenberger, D. J., de Groot, T. E., Wan, A. M. D., Beebe, D. J., Young, E. W. K., *Lab Chip* 2015, *15*, 2364–2378.

[36] Islam, M., Natu, R., Martinez-Duarte, R., *Microfluid. Nanofluid.* 2015, *19*, 973–985.

[37] Nuzaihan M. N. M., Hashim, U., Rahim Ruslinda, A., Md Arshad, M. K., Baharin, M. H. A., *Curr. Nanosci.* 2015, *11*, 239–244.

[38] Picollo, F., Battiato, A., Boarino, L., Ditalia Tchernij, S., Enrico, E., Forneris, J., Gilardino, A., Jakšić, M., Sardi, F., Skukan, N., Tengattini, A., Olivero, P., Re, A., Vittone, E., *Nucl. Instrum. Methods Phys. Res. Sect. B* 2017, *404*, 193–197.

[39] Bhattacharjee, N., Urrios, A., Kang, S., Folch, A., *Lab Chip* 2016, *16*, 1720–1742.

[40] Ngo, T. D., Kashani, A., Imbalzano, G., Nguyen, K. T. Q., Hui, D., *Compos. Part B Eng.* 2018, *143*, 172–196.

[41] Lapizco-Encinas, B. H., Simmons, B. A., Cummings, E. B., Fintschenko, Y., *Anal. Chem.* 2004, *76*, 1571–1579.

[42] Moncada-Hernandez, H., Baylon-Cardiel, J. L., Pérez-González, V. H., Lapizco-Encinas, B. H., *Electrophoresis* 2011, *32*, 2502–2511.

[43] Gallo-Villanueva, R. C., Rodríguez-López, C. E., Díaz-de-la-Garza, R. I., Reyes-Betanzo, C., Lapizco-Encinas, B. H., *Electrophoresis* 2009, *30*, 4195–4205.

[44] Nakano, A., Camacho-Alanis, F., Ros, A., *Analyst* 2015, *140*, 860–868.

[45] Gallo-Villanueva, R. C., Jesús-Pérez, N. M., Martínez-López, J. I., Pacheco, A., Lapizco-Encinas, B. H., *Microfluid. Nanofluid.* 2011, *10*, 1305–1315.

[46] Ayala-Mar, S., Perez-Gonzalez, V. H., Mata-Gómez, M. A., Gallo-Villanueva, R. C., González-Valdez, J., *Anal. Chem.* 2019, *91*, 14975–14982.

[47] Green, N. G., Morgan, H., *J. Phys. Chem. B* 1999, *103*, 41–50.

[48] Perez-Gonzalez, V. H., Gallo-Villanueva, R. C., Cardenas-Benitez, B., Martinez-Chapa, S. O., Lapizco-Encinas, B. H., *Anal. Chem.* 2018, *90*, 4310–4315.

[49] Zhao, H., *Electrophoresis* 2011, *32*, 2232–2244.

[50] Srivastava, S. K., Baylon-Cardiel, J. L., Lapizco-Encinas, B. H., Minerick, A. R., *J. Chromatogr. A* 2011, *1218*, 1780–1789.

[51] LaLonde, A., Gencoglu, A., Romero-Creel, M. F., Koppula, K. S., Lapizco-Encinas, B. H., *J. Chromatogr. A* 2014, *1344*, 99–108.

[52] Kaler, K. V, Jones, T. B., *Biophys. J.* 1990, *57*, 173–182.

[53] Urdaneta, M., Smela, E., *Electrophoresis* 2007, *28*, 3145–3155.

[54] Mohammadi, M., Madadi, H., Casals-Terré, J., Sellarès, J., *Anal. Bioanal. Chem.* 2015, *407*, 4733–4744.

[55] Hill, N., Lapizco-Encinas, B. H., *Anal. Bioanal. Chem.* 2020, *412*, 3891–3902.

[56] Gallo-Villanueva, R. C., Pérez-González, V. H., Davalos, R. V., Lapizco-Encinas, B. H., *Electrophoresis* 2011, *32*, 2456–2465.

[57] Moncada-Hernandez, H., Nagler, E., Minerick, A. R., *Electrophoresis* 2014, *35*, 1803–1813.

[58] Pethig, R., *J. Electrochem. Soc.* 2016, *164*, B3049–B3055.

[59] Davalos, R. V., McGraw, G. J., Wallow, T. I., Morales, A. M., Krafcik, K. L., Fintschenko, Y., Cummings, E. B., Simmons, B. A., *Anal. Bioanal. Chem.* 2008, *390*, 847–855.

[60] Hill, N., Lapizco-Encinas, B. H., *Electrophoresis* 2019, *40*, 2541–2552.

[61] Saucedo-Espinosa, M. A., Lapizco-Encinas, B. H., *J. Chromatogr. A* 2015, *1422*, 325–333.

[62] Nakano, A., Luo, J., Ros, A., *Anal. Chem.* 2014, *86*, 6516–6524.

[63] Swami, N., Chou, C.-F., Ramamurthy, V., Chaurey, V., *Lab Chip* 2009, *9*, 3212–3220.

[64] Chaurey, V., Rohani, A., Su, Y.-H., Liao, K.-T., Chou, C.-F., Swami, N. S., *Electrophoresis* 2013, *34*, 1097–1104.

[65] Rohani, A., Moore, J. H., Kashatus, J. A., Sesaki, H., Kashatus, D. F., Swami, N. S., *Anal. Chem.* 2017, *89*, 5757–5764.

[66] Moore, J. H., Honrado, C., Stagnaro, V., Kolling, G., Warren, C. A., Swami, N. S., *ACS Infect. Dis.* 2020, *6*, 1000–1007.

[67] Jones, P. V, Salmon, G. L., Ros, A., *Anal. Chem.* 2017, *89*, 1531–1539.

[68] Luo, J., Abdallah, B. G., Wolken, G. G., Arriaga, E. A., Ros, A., *Biomicrofluidics* 2014, *8*, 21801.

[69] Gan, L., Chao, T.-C., Camacho-Alanis, F., Ros, A., *Anal. Chem.* 2013, *85*, 11427–11434.

[70] Wang, Q., Dingari, N. N., Buie, C. R., *Electrophoresis* 2017, *38*, 2576–2586.

[71] Pysher, M. D., Hayes, M. A., *Anal. Chem.* 2007, *79*, 4552–4557.

[72] Jones, P. V, DeMichele, A. F., Kemp, L., Hayes, M. A., *Anal. Bioanal. Chem.* 2014, *406*, 183–192.

[73] Ding, J., Lawrence, R. M., Jones, P. V, Hogue, B. G., Hayes, M. A., *Analyst* 2016, *141*, 1997–2008.

[74] Liu, Y., Hayes, M. A., *Anal. Chem.* 2021, *93*, 1352–1359.

[75] Sano, M. B., Gallo-Villanueva, R. C., Lapizco-Encinas, B. H., Davalos, R. V., *Microfluid. Nanofluid.* 2013, *15*, 599–609.

[76] Salmanzadeh, A., Romero, L., Shafiee, H., Gallo-Villanueva, R. C., Stremler, M. A., Cramer, S. D., Davalos, R. V., *Lab Chip* 2012, *12*, 182–189.

[77] Henslee, E. A., Sano, M. B., Rojas, A. D., Schmelz, E. M., Davalos, R. V., *Electrophoresis* 2011, *32*, 2523–2529.

[78] Hanson, C., Barney, J. T., Bishop, M. M., Vargis, E., *Electrophoresis* 2019, *40*, 1446–1456.

[79] Shafiee, H., Sano, M. B., Henslee, E. A., Caldwell, J. L., Davalos, R. V., *Lab Chip* 2010, *10*, 438–445.

[80] Kale, A., Malekanfard, A., Xuan, X., *Micromachines* 2020, *11*, 707.

[81] Zhu, J., Xuan, X., *J. Colloid Interface Sci.* 2009, *340*, 285–290.

[82] Zhu, J., Canter, R. C., Keten, G., Vedantam, P., Tzeng, T.-R. J., Xuan, X., *Microfluid. Nanofluid.* 2011, *11*, 743–752.

[83] Patel, S., Qian, S., Xuan, X., *Electrophoresis* 2013, *34*, 961–968.

[84] Harrison, H., Lu, X., Patel, S., Thomas, C., Todd, A., Johnson, M., Raval, Y., Tzeng, T.-R., Song, Y., Wang, J., Li, D., Xuan, X., *Analyst* 2015, *140*, 2869–2875.

[85] Braff, W. A., Pignier, A., Buie, C. R., *Lab Chip* 2012, *12*, 1327–1331.

[86] Wang, Q., Jones, A.-A. D., Gralnick, J. A., Lin, L., Buie, C. R., *Sci. Adv.* 2019, *5*, eaat5664.

[87] Braff, W. A., Willner, D., Hugenholtz, P., Rabaey, K., Buie, C. R., *PLoS One* 2013, *8*, e76751.

[88] LaLonde, A., Romero-Creel, M. F., Lapizco-Encinas, B. H., *Electrophoresis* 2015, *36*, 1479–1484.

[89] Bhattacharya, S., Chao, T.-C., Ariyasinghe, N., Ruiz, Y., Lake, D., Ros, R., Ros, A., *Anal. Bioanal. Chem.* 2014, *406*, 1855–1865.

[90] Crowther, C. V, Hilton, S. H., Kemp, L., Hayes, M. A., *Anal. Chim. Acta* 2019, *1068*, 41–51.

[91] Liu, Y., Jiang, A., Kim, E., Ro, C., Adams, T., Flanagan, L. A., Taylor, T. J., Hayes, M. A., *Analyst* 2019, *144*, 4066–4072.

[92] Ding, J., Woolley, C., Hayes, M. A., *Anal. Bioanal. Chem.* 2017, *409*, 6405–6414.

[93] Tada, S., Eguchi, M., Okano, K., *Electrophoresis* 2019, *40*, 1494–1497.

[94] Malekanfard, A., Beladi-Behbahani, S., Tzeng, T.-R., Zhao, H., Xuan, X., *Anal. Chem.* 2021, *93*, 5947–5953.

[95] Cho, Y.-K., Kim, S., Lee, K., Park, C., Lee, J.-G., Ko, C., *Electrophoresis* 2009, *30*, 3153–3159.

[96] Zellner, P., Shake, T., Hosseini, Y., Nakidde, D., Riquelme, M. V, Sahari, A., Pruden, A., Behkam, B., Agah, M., *Electrophoresis* 2015, *36*, 277–283.

[97] Lewpiriyawong, N., Yang, C., Lam, Y. C., *Microfluid. Nanofluid.* 2012, *12*, 723–733.

[98] Lozada-Cassou, M., González-Tovar, E., Olivares, W., *Phys. Rev. E: Stat. Phys. Plasmas Fluids Relat. Interdiscip. Top.* 1999, *60*, R17–R20.

[99] Ben, Y., Demekhin, E. A., Chang, H.-C., *J. Colloid Interface Sci.* 2004, *276*, 483–497.

[100] Mishchuk, N. A., Barinova, N. O., *Colloid J.* 2011, *73*, 88–96.

[101] Barany, S., Madai, F., Shilov, V., *Study of nonlinear electrophoresis*, Springer, Berlin 2004, pp. 14–20.

[102] Figliuzzi, B., Chan, W. H. R., Moran, J. L., Buie, C. R., *Phys. Fluids* 2014, *26*, 102002.

[103] Bazant, M. Z., Squires, T. M., *Curr. Opin. Colloid Interface Sci.* 2010, *15*, 203–213.

[104] Bazant, M. Z., Kilic, M. S., Storey, B. D., Ajdari, A., *Adv. Colloid Interface Sci.* 2009, *152*, 48–88.

[105] Saucedo-Espinosa, M. A., Lapizco-Encinas, B. H., *Biomicrofluidics* 2016, *10*, 33104.

[106] Sureda, M., Miller, A., Diez, F. J., *Electrophoresis* 2012, *33*, 2759–2768.

[107] Devasenathipathy, S., Santiago, J. G., Takehara, K., *Anal. Chem.* 2002, *74*, 3704–3713.

[108] Schnitzer, O., Yariv, E., *Phys. Fluids* 2014, *26*, 122002.

[109] Schnitzer, O., Zeyde, R., Yavneh, I., Yariv, E., *Phys. Fluids* 2013, *25*, 52004.

[110] Tottori, S., Misiunas, K., Keyser, U. F., Bonthuis, D. J., *Phys. Rev. Lett.* 2019, *123*, 14502.

[111] Yariv, E., *Europhys. Lett.* 2008, *82*, 54004.

[112] Coll De Peña, A., Miller, A., Lentz, C. J., Hill, N., Parthasarathy, A., Hudson, A. O., Lapizco-Encinas, B. H., *Anal. Bioanal. Chem.* 2020, *412*, 3935–3945.

[113] Coll De Peña, A., Hill, N., Lapizco-Encinas, B. H., *Biosensors* 2020, *10*, 148.

[114] Quevedo, D. F., Lentz, C. J., Coll de Peña, A., Hernandez, Y., Habibi, N., Miki, R., Lahann, J., Lapizco-Encinas, B. H., *Beilstein J. Nanotechnol.* 2020, *11*, 1556–1567.

[115] Antunez-Vela, S., Perez-Gonzalez, V. H., De Peña, A. C., Lentz, C. J., Lapizco-Encinas, B. H., *Anal. Chem.* 2020, *92*, 14885–14891.

[116] Prabhakaran, R. A., Zhou, Y., Patel, S., Kale, A., Song, Y., Hu, G., Xuan, X., *Electrophoresis* 2017, *38*, 572–579.

[117] Sridharan, S., Zhu, J., Hu, G., Xuan, X., *Electrophoresis* 2011, *32*, 2274–2281.

[118] Kale, A., Song, L., Lu, X., Yu, L., Hu, G., Xuan, X., *Electrophoresis* 2018, *39*, 887–896.

[119] Malekanfard, A., Liu, Z., Song, L., Kale, A., Zhang, C., Yu, L., Song, Y., Xuan, X., *Electrophoresis* 2021, *42*, 626–634.

[120] Xuan, X., *Electrophoresis* 2022, *43*, DOI: https://doi.org/10.1002/elps.202100090.

[121] Ramirez-Murillo, C. J., de los Santos-Ramirez, J. M., Perez-Gonzalez, V. H., *Electrophoresis* 2021, *42*, 565–587.

